BIOCHEMISTRY
including biophysical chemistry & molecular biology

Article

pubs.acs.org/biochemistry

Allosteric Reversion of *Haemophilus influenzae* β-Carbonic Anhydrase via a Proline Shift

Katherine M. Hoffmann,[†,‡] H. Rachael Million-Perez,[‡] Richard Merkhofer,[‡] Hilary Nicholson,[‡] and Roger S. Rowlett*[,‡]

[†]Department of Chemistry, Gonzaga University, 502 East Boone Avenue, Spokane, Washington 99258, United States
[‡]Department of Chemistry, Colgate University, 13 Oak Drive, Hamilton, New York 13346, United States

ABSTRACT: *Haemophilus influenzae* β-carbonic anhydrase (HICA) has been reverse-engineered in the allosteric site region to resemble the nonallosteric *Pisum sativum* enzyme in order to identify critical features of allostery and intersusbunit communication. Three variants (W39V/G41A, P48S/A49P, and W39V/G41A/P48S/A49P) were identified, through a comparison with a crystal structure of nonallosteric *P. sativum* β-carbonic anhydrase (PSCA, PDB 1EKJ), to potentially revert HICA to a nonallosteric enzyme. The W39V/G41A and P48S/A49P mutations decreased the apparent k_{cat}/K_m proton dependence from 4 to 2 and 1, respectively, increasing the overall maximal k_{cat}/K_m to 16 ± 2 μM^{-1} s^{-1} (380% of wild type) and 17 ± 3 μM^{-1} s^{-1} (405% of wild type). The pK_a values of the metal-bound water molecule based on the pH−rate profile kinetics (8.32 ± 0.04 for W39V/G41A and 8.3 ± 0.1 for P48S/A49P) were also slightly higher than that for the wild-type enzyme (7.74 ± 0.04). The P48S/A49P variant has lost all pH−rate cooperativity. The W39V/G41A/P48S/A49P variant's kinetics were unusual and were fit with a log−linear function with a slope 0.9 ± 0.2. The crystal structure of the W39V/G41A variant revealed an active site very similar to the T-state wild-type oligomer with bicarbonate trapped in the escort site. By contrast, the X-ray crystal structure of a proline shift variant (P48S/A49P) reveals that it has adopted an active site conformation nearly identical to that of nonallosteric β-carbonic anhydrase (R-state) for one chain, including a tight association with the dimer-exchanged N-terminal helices; the second chain in the asymmetric unit is associated in a biologically relevant oligomer, but it adopts a T-state conformation that is not capped by dimer-exchanged N-terminal helices. The hybrid R/T nature of HICA P48S/A49P structurally recapitulates the interruption of pH−rate cooperativity observed for this variant. Comparison of the conformations of the R and T chains of P48S/A49P suggests a new hypothesis to explain HICA allosteric communication that is mediated by the N-terminal helices and anion binding at the dimer interface.

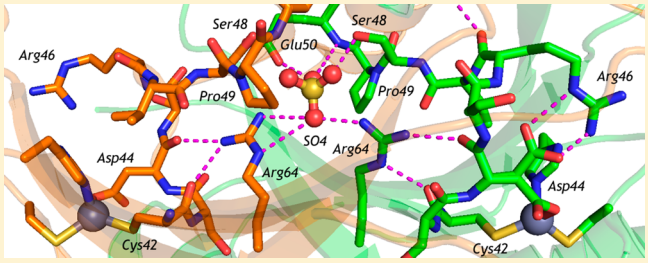

Carbonic anhydrases (CA; carbonate hydrolyase, EC 4.2.1.1) are metalloenzymes that catalyze the interconversion of CO_2 and bicarbonate:

$$CO_2 + H_2O \rightleftarrows HCO_3^- + H^+ \quad (1)$$

To date, there are five known convergently evolved forms of the enzyme (α–ζ).[1−5] The β-form is broadly distributed in nature, including bacteria, yeast, plant chloroplasts, and invertebrates.[2,6] In bacteria, it is believed to be an accessory enzyme for carboxylases involved in fatty acid synthesis.[7] Despite the lack of an evolutionary common ancestor, most CAs are active as zinc−metalloenzymes, although the γ- and ζ-forms can utilize Fe^{2+}[8] and Cd^{2+},[9] respectively, and Co^{2+} has been used as a spectroscopically active mimic of Zn^{2+}.[10−16] X-ray crystallography[9,17−21] and/or EXAFS[122] reveals further that most CA forms share a similar four-coordinate metal ion coordination sphere of the type $His_3(H_2O)$ or $Cys_2His(H_2O)$, where the ionizable water ligand presumably serves an essential role in the catalytic mechanism.

Within a single form of CAs, the fold of the protein is generally conserved, although the order of secondary structure elements can vary. The active sites in the β-CAs can be capped by distal portions of the protein, sometimes by helices contributed by a dimer partner: in *Porphyridium purpureum* β-CA (PDB 1DDZ), three N-terminal helices fold back over the central twisted β-sheet from the other side of the protein.[20] In *Pisum sativum* (PSCA, PDB 1EKJ) and *Haemophilus influenzae* β-CA (HICA, PDB 2A8C), two N-terminal helices and two loops from one chain fold over the active sites of the dimer partner.[17,19] It may be, however, that the N-termini in the β-CA fold are flexibly associated with the globular fold of the protein; many variants of HICA frequently exhibit disordered N-terminal residues.[23,24] Additionally, the *Methanobacterium thermoautotrophicum* β-CA (PDB 1G5C) domain swaps its N-terminal helix with an independent neighbor in the crystal lattice, an artifact of crystallization that may argue for a flexible set of positions for N-termini in β-CAs.[21]

Received: September 3, 2014
Revised: December 11, 2014
Published: December 15, 2014

DOI: 10.1021/bi501116e
Biochemistry 2015, 54, 598−611

Scheme 1. Structural Schematic of Key Active Site and Noncatalytic Bicarbonate Binding Site Interactions in the Hypothesized Active (R-State) and Inactive (T-State) Conformations of HICA[17]

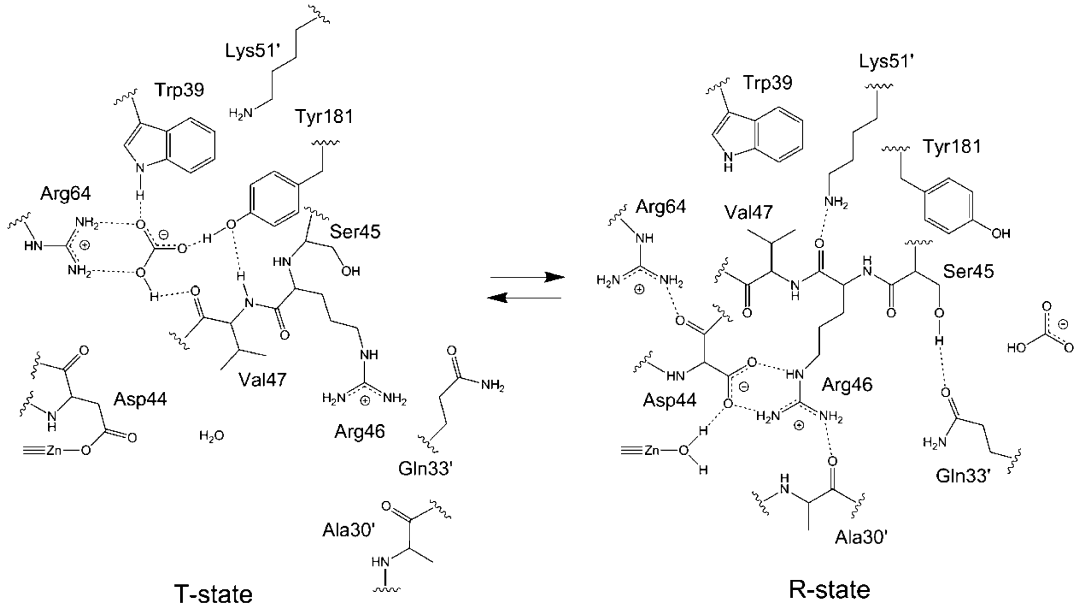

X-ray crystallographic analysis of β-CAs revealed two distinct subclasses of this enzyme form based on active site organization.[25,26] One subclass, exemplified by the structures of enzymes from *P. sativum*, *M. thermoautotrophicum*, and *Mycobacterium tuberculosis* Rv1284 (PDB 1YLK), has the canonical open $Cys_2His(H_2O)$ zinc coordination site. The other subclass of β-CAs, exemplified by structures the enzymes from *H. influenzae*, *Escherichia coli* (PDB 1I6P), *P. purpureum*, and *M. tuberculosis* Rv3588c (PDB 1YM3), has a unique zinc coordination geometry, where the catalytically essential water molecule has been replaced by an Asp residue, resulting in a closed $Cys_2HisAsp$ coordination sphere.

Consistent with the structural differences in X-ray crystal structures, there is also a functional difference between β-CAs that adopt the open and closed active site structures. Kinetics studies of plant and bacterial β-CA[17,27−31] show that both subclasses of enzyme are highly efficient catalysts for the CO_2 hydration reaction (eq 1), with k_{cat} values on the order of 10^5 s^{-1} and k_{cat}/K_m values on the order of 10^8 M^{-1} s^{-1}. HICA, which crystallizes in a closed β-CA structure, has been shown to have highly cooperative pH−rate profiles for k_{cat} and k_{cat}/K_m and to exhibit cooperative inhibition by HCO_3^-.[17] In addition, X-ray crystallographic studies of both HICA (PDB 2A8D) and *E. coli* β-CA (ECCA, PDB 2ESF) reveal a noncatalytic binding site for bicarbonate ion, and a few structures, notably, HICA (PDB 2A8D) and *Streptomyces mutans* β-CA (PDB 3LAS), have an anion binding site at the dimerization interface. In contrast to HICA, β-CAs with open active site conformations that have been thoroughly kinetically characterized are not inhibited by HCO_3^- and do not exhibit cooperative pH−rate profiles. Therefore, it has been hypothesized that HICA and perhaps other β-CAs with a closed active site represent an allosteric form of CA, in which the observed X-ray crystallographic structures probably represent the inactive, T-state,[32] conformation of the enzyme.[17] Presumably, the active R-state[32] of these allosterically regulated β-CAs resembles the crystal structures of the nonallosteric β-CAs. Kinetic evidence suggests that the fundamental allosteric unit is a dimer, not a tetramer.[17] The allosteric dimer is characterized by the protein chains that mutually wrap their N-terminal helices around one another and has an interaction interface over 7000 Å^2 in area. Two allosteric dimers interact through a smaller, weaker tetramerization interface of about 3000 Å^2 in area to form the tetrameric holoenzyme.

A structural comparison of the allosteric HICA to non-allosteric *P. sativum* enzyme (PSCA)[25] reveals that the coordination of Asp44 to zinc (in HICA) not only displaces the catalytically essential water molecule and metal ion but also a hydrogen-bond network that involves a bidentate Asp44−Arg46 salt bridge, which continues to a the backbone carbonyl of Ala30′ on the neighboring chain. (Note that residue numbers reference *H. influenzae* β-CA unless otherwise indicated; residue numbers with a prime reference residues on the neighboring chain of the allosteric dimer.) The loop containing Ala30′ caps the active site access and additionally recruits Gln33′, which likely donates a hydrogen bond to the metal-bound bicarbonate ion during catalysis.[33] The activation loop, defining the entrance point for inhibitory anions (escort site),[23] the binding pocket (allosteric pocket), and active site, differs significantly between HICA and PSCA in only a few locations: In PSCA, Trp39 (HICA) is replaced by a valine (PSCA) at the top of the activation loop; on the side of the allosteric pocket, Pro48 (HICA) is shifted one residue later in sequence in PSCA, and Gly41 (HICA) is replaced by the a bulkier alanine residue in PSCA.

The enzyme activity of HICA and related allosteric β-CAs are believed to be regulated by a simple ligand exchange mechanism where Asp44 displaces the catalytically essential water molecule in the fourth ligand position of the metal ion. A diagram depicting key features in this mechanism is shown in Scheme 1. A key event in this structural transition is the reorientation of the activation loop, residues 44−51. The T-state conformation, represented by Asp44 bound to the metal ion, is stabilized by the binding of HCO_3^- in the allosteric pocket, an instance of product inhibition, requiring entrance through an escort site defined by Arg64 and Glu50 from each of the two protein chains at the dimer interface. Inhibitory bicarbonate interacts with Trp39, Arg64, Tyr181 and the main

DOI: 10.1021/bi501116e
Biochemistry 2015, 54, 598−611

chain carbonyl oxygen of Val47 in the allosteric pocket. The side chain of Val47 has been implicated to play a critical role in displacing the noncatalytic HCO_3^- ion in the R-state, repositioning Asp44 to coordinate to the metal ligand.[17] The activation loop is in proximity to helix 1 and helix 2 from the neighboring protein chain and packs against helix 3. The three-dimensional orientation of the active site, activation loop, allosteric site, escort site, and N-terminal helices in wild-type HICA is depicted in Figure 1.

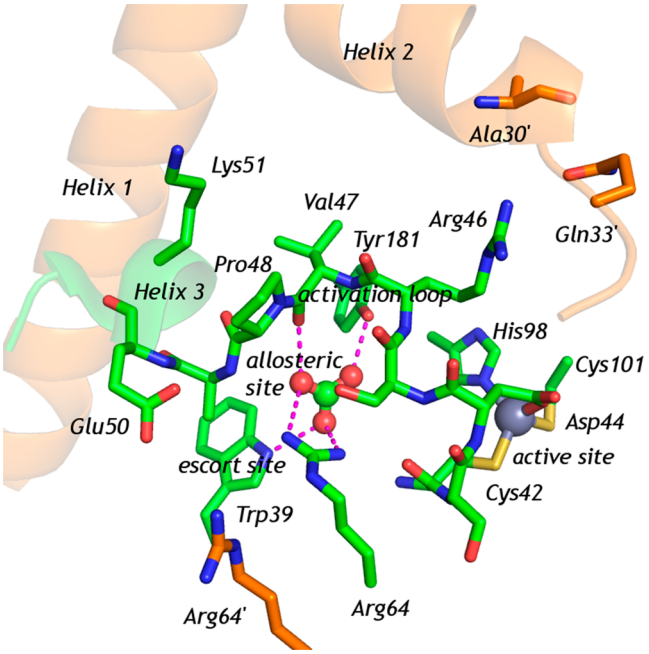

Figure 1. Orientation of key structural elements in the allosteric dimer of HICA, based on PDB 2A8D. This figure depicts the T-state of the enzyme as shown in Scheme 1. The main chain of the allosteric dimer is shown in green. The neighboring chain of the allosteric dimer is shown in orange. Helix 1 is composed of residues 1−21 of the neighboring chain. Helix 2 is composed of residues 24−32 of the neighboring chain. The C-terminus of helix 2 and Gln33′ cap the active site of the enzyme. Helix 3 is composed of residues 50−54. Bicarbonate ion is shown bound to the allosteric site, which includes the coordinating residues Trp39, Arg64, and Tyr 181. The escort site is an anion binding site that forms the entrance to the allosteric site and is solvent-accessible in the dimerization interface. It is composed of Arg64 and Glu50 from each chain of the allosteric dimer (Glu50′ has been omitted for clarity.). The activation loop is composed of residues 44−51. The active site contains the metal ligands Cys42, Cys101, and His98 as well as (in the T-state) Asp44.

Structures of HICA have crystallized almost entirely in the T-state conformation, which seems to be the default regardless of pH or inhibitory bicarbonate concentration. The existence of an R-state for HICA is inferred from the observed catalytic kinetics, which is similar to other β-CAs. The likely structure of the R-state is assumed to be similar to the structures of the other, nonallosteric structural subclass of β-CA such as PSCA, a thiocyanate inhibitor complex of *M. tuberculosis* β-CA in which the inhibitor has displaced the Asp ligand,[34] and a catalytically inactive HICA-D44N variant that crystallizes in an R-like state conformation, with Asn44 flipped away from the zinc ligand and replaced by a water molecule.[24] The HICA-D44N variant is not catalytically active, and the hydrogen-bond interaction between Arg46 and Ala30′ is not ordered; however, the backbone around the active site and activation loop was remarkably identical to PSCA.[25]

We have previously shown that partially reverse-engineered single variants HICA-G41A and -W39F are not sufficient to abolish pH−rate cooperativity or bicarbonate inhibition in HICA,[23,24] although they did trap inhibitory bicarbonate in the escort site. However, the P48S/A49P variant should impose severe steric constraints for bicarbonate binding in the allosteric site, as the backbone position should redirect the proline ring directly into the allosteric pocket.[24] Therefore, the proline shift variant has the potential to destabilize the T-state of the enzyme by preventing bicarbonate access, potentially allowing direct investigation of the R-state of HICA.

We therefore constructed the HICA proline shift variant P48S/A49P, which mimics *P. sativum* β-CA at this position in the protein sequence. Additionally, we examined the double variant W39V/G41A as well as a quadruple variant W39V/G41A/P48S/A49P to examine which, if any, of these structural features are sufficient to disrupt cooperativity in HICA and stabilize the protein in an R-state conformation.

We found that the double variant HICA-G41A/W39V is catalytically competent and isostructural with wild-type HICA, except that bicarbonate does not bind in the allosteric site and is trapped instead in the anion binding site we have previously termed the escort site.[23] The quadruple variant, which is most similar in sequence to the PSCA activation loop, is catalytically anomalous, suggesting an unanticipated destabilization not accounted for in the variant design. The HICA-P48S/A49P variant is catalytically competent and appears to have lost pH−rate cooperativity in the CO_2 hydration reaction. Furthermore, the X-ray crystal structure of HICA-P48S/A49P directly reveals the loss of cooperativity, presenting an R-state equilibrium in one active site of the allosteric dimer (with complete hydrogen-bond network through Arg46 and the capping Ala30′ loop) and a T-state conformation in the other active site. The proline shift of HICA-P48S/A49P significantly repositions helix 3, which interacts with the escort site, allosteric site, and activation loop. With no other shifts in the activation loop, this suggests that the ordered N-terminal helices packing against helix 3 may be important for intersubunit communication and R-state conformation stabilization of the active site. Additionally, the P48S/A49P structure also suggests a potentially important role for the escort site anion in stabilizing helix 3 and therefore the R-state. We conclude that the proline shift HICA P48S/A49P variant is sufficient for complete reversion of allostery for a β-CA and represents the first time two distinct active site conformations have been simultaneously observed in a catalytically competent β-CA.

EXPERIMENTAL PROCEDURES

Expression and Purification of Recombinant Enzymes. Site-directed mutations were constructed using megaprimer PCR[35] with *Pfu* ultra (Stratagene) polymerase and commercial oligonucleotides (Integrated DNA Technologies). For mutation W39V/G41A, a mutant oligonucleotide, 5′-AGCA**AGC**AAT**CAC**AAGGTAATGTGG-3′, was paired with the 5′ oligonucleotide primer PHI1X (5′-TGCCCATGGA-TAAAATTAAACAACTCTTT-3) over the previously constructed G41A HICA plasmid[24] in the first PCR reaction to give a 129 bp product. (Mutation sites of oligonucleotides are in bold; restriction endonuclease sites for cloning are underlined.) This PCR product was used as a megaprimer in a second PCR reaction with the 3′ oligonucleotide primer

DOI: 10.1021/bi501116e
Biochemistry 2015, 54, 598−611

Table 1. Data Collection and Refinement Statistics for HICA Variants[a]

	W39V/G41A + 500 mM HCO_3^- (PDB 4WAK)	W39V/G41A/P48S/A49P (PDB 4WAM)	P48S/A49P (PDB 4WAJ)
data collection statistics			
wavelength (Å)	1.54	1.54	1.54
space group	$I2_12_12_1$	$I2_12_12_1$	$P4_12_12$
cell parameters			
cell edges (Å)	144.67, 129.01	48.16, 130.26, 143.87	82.78, 82.78, 186.50
angles (deg)	48.33, 90, 90, 90	90, 90, 90	90, 90, 90
resolution (Å)	29.5−2.49 (2.59−2.49)	29.8−2.20 (2.26−2.20)	29.2−2.70 (2.77−2.70)
unique reflections	16 109 (1613)	22 403 (1173)	18 148 (1177)
redundancy	9.6 (5.8)	3.3 (2.1)	5.9 (4.1)
completeness	98.5 (99.6)	95.3 (83.1)	97.9 (99.3)
R_{sym} (%)	0.127 (0.488)	0.101 (0.521)	0.074 (0.356)
$\langle I\rangle/\langle\sigma I\rangle$[b]	15.1 (1.5)	7.2 (1.7)	19.3 (2.1)
reflections in test set	817	1164	931
R_{work} (%)	18.5	23.2	16.1
R_{free} (%)	25.4	28.7	23.2
no. of atoms (average B-factor, Å^2)			
protein	2793 (37.7)	2843 (26.1)	3214 (47.5)
ion	11 (42.9)	22 (34.1)	22 (55.6)
solvent	101 (27.8)	144 (27.7)	71 (29.5)
rmsd from ideal[c]			
bond distance (Å)	0.014	0.016	0.014
bond angle (deg)	1.59	1.79	1.70
Ramachandran plot outliers (%)[d]	0.59	0.58	0.76

[a]Values in parentheses represent data for the highest resolution shell. [b]Reported as $\langle\langle I\rangle/\sigma\langle I\rangle\rangle$ in SCALA or SCALEPACK. [c]Ideal values from Engh and Huber.[47] [d]Calculated using a strict boundary Ramachandran plot.[45]

PHI2X (5′-TGCCTGCAGTTATTATGTATTTTCAAGATG-3′) to create the final mutated HICA gene. The final PCR product was used as a megaprimer in a MEGAWHOP[36] PCR protocol. Variant P48S/A49P was constructed similarly using the mutant oligonucleotide 5′- GTCAATTTTTC**AGGAGA**C-ACACGGCT-3′. For variant W39V/G41A/P48S/A49P, the mutant oligonucleotide for P48S/A49P was used with the W39V/G41A plasmid to create the quadruple mutant. All expression plasmids were subjected to DNA sequencing (PE Biosystems ABI 310, BigDye 3.0 chemistry) of the entire HICA gene to verify introduction of the correct mutations.

Expression, purification, storage, and quantification of variants and Co(II)-substituted HICA was as described previously.[16,24] Briefly, crude homogenates of overexpressed protein were purified to homogeneity by ion exchange (Q-Sepharose FF), hydrophobic interaction (butylsepharose FF), and gel exclusion chromatography (Superdex 200) using an AKTA FPLC (GE Healthcare). All proteins were quantified by ICP-OES (PerkinElmer Optima SC 3000) for zinc at 213.856 nm and cobalt at 228.616 nm, as applicable. The concentration of Co(II)-substituted P48S/A49P for spectroscopic data was based on total cobalt concentration.

Steady-State Kinetics Methods. Saturated solutions of CO_2 were prepared by bubbling CO_2 gas into water in a vessel maintained at 25.0 ± 0.1 °C, and dilutions were prepared in the absence of air by coupling two gastight syringes as described by Khalifah.[37] CO_2 concentrations were calculated based on a 33.8 mM saturated solution at 25.0 °C.[38]

All steady-state kinetic measurements were made at 25.0 °C using a Hi-Tech SF-61DX2 stopped-flow spectrophotometer. Initial rates of CO_2 hydration were measured using the changing pH indicator method described previously.[37−39] All pH−profile kinetic studies were carried out in the presence of 250 mM Na_2SO_4, for maximum enzyme stability and activity in dilute solution,[17] except where noted. The pH−rate profiles of k_{cat} and k_{cat}/K_m were fit to eqs 2, 3, or 4.[17] Equation 2 describes a pH dependence that requires the cooperative loss of two protons to generate the active enzyme, where k_{obs} is the observed value of k_{cat} or k_{cat}/K_m, k_{max} is the maximal value of k_{cat} or k_{cat}/K_m, and K_a corresponds to the dissociation constants for the cooperative ionization of the enzyme, $EH_2 \leftrightarrows E^{2-} + 2\,H^+$, where the doubly deprotonated form of the enzyme is the active species.

$$k_{obs} = \frac{k_{max}}{\left(1 + \frac{[H^+]^2}{K_a^2}\right)} \quad (2)$$

Equation 3 describes a pH dependence that requires the cooperative loss of four protons with identical pK_a values to generate the active enzyme species, i.e., $EH_4 \leftrightarrows E^{4-} + 4H^+$, where E^{4-} is the active species of enzyme and k_{max} is the maximal value of k_{cat} or k_{cat}/K_m.

$$k_{obs} = \frac{k_{max}}{\left(1 + \frac{[H^+]^4}{K_a^4}\right)} \quad (3)$$

Equation 4 describes a pH dependence that requires the loss of a single proton with a pK_a value to generate the active enzyme species, i.e., $EH \leftrightarrows E^- + H^+$, where E^- is the active species of enzyme and k_{max} is the maximal value of k_{cat} or k_{cat}/K_m.

$$k_{obs} = \frac{k_{max}}{\left(1 + \frac{[H^+]}{K_a}\right)} \quad (4)$$

DOI: 10.1021/bi501116e
Biochemistry 2015, 54, 598−611

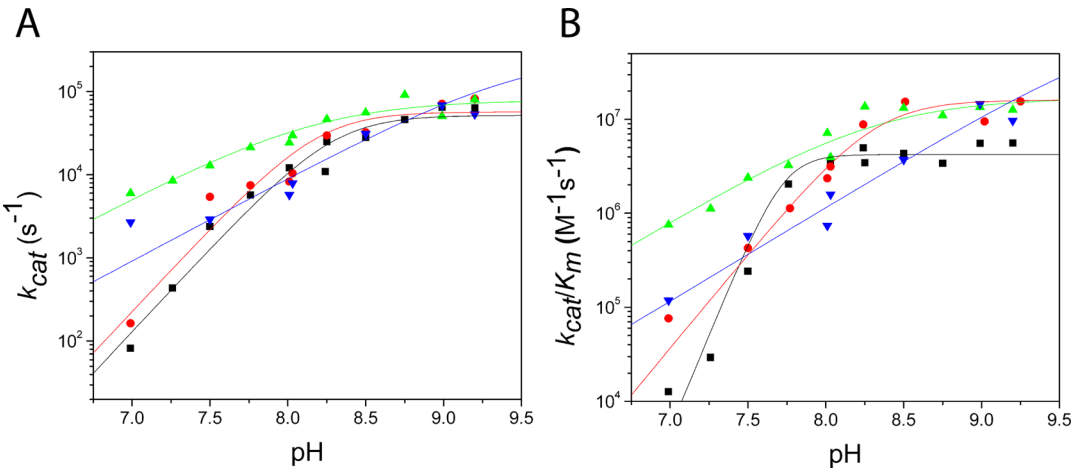

Figure 2. Cooperative steady-state pH−rate profiles of (A) k_{cat} and (B) k_{cat}/K_m for HICA (black squares) and variants W39V/G41A (red circles), P48S/A49P (green triangles), W39V/G41A/P48S/A49P (blue triangles). (A) Fit to eq 3 with k_{max} = 69 ± 29 ms^{-1} and pK_a = 8.3 ± 0.6 (wild type) and k_{max} = 57 ± 20 ms^{-1} and pK_a = 8.2 ± 0.1 (W39V/G41A) and fit to eq 4 with k_{max} = 79 ± 10 ms^{-1} and pK_a = 8.17 ± 0.09 (P48S/A49P) and a log−linear model with slope = 1.7 ± 0.8 (W39V/G41A/P48S/A49P). (B) Fit to eq 2 with k_{max} = 4.3 ± 0.8 μM^{-1} s^{-1}, pK_a = 7.74 ± 0.04 (wild type); eq 3 with k_{max} = 16 ± 2 μM^{-1} s^{-1} and pK_a 8.32 ± 0.04 (W39V/G41A); and eq 4 with k_{max} = 17 ± 3 μM^{-1} s^{-1} and pK_a = 8.3 ± 0.1 (P48S/A49P); and a log−linear model with slope = 0.9 ± 0.2 (W39V/G41A/P48S/A49P). Reactions were carried out at 25 °C in 40 mM buffer (1-methylimidazole, pH 7.0−8.25; 1,2-dimethylimidazole, pH 8.25−9.25), 30−200 μM indicator dye (*p*-nitrophenol with 1-methylimidazole; m-cresol purple with 1,2-dimethylimidazole), 10 μM EDTA, 250 mM Na_2SO_4, and 1−2 μM enzyme.

Experimental data for k_{cat} and k_{cat}/K_m were fit to the logarithmic forms of eqs 2−4 using nonlinear least-squares in Origin 7.0 (Microcal) and represent analyses of data from at least three replicate measurements. Values of k_{cat} and k_{cat}/K_m are reported here on a per subunit basis.

The sulfate-dependent variation of the rate of the enzyme-catalyzed CO_2 hydration reaction was performed similarly using 8.45 mM CO_2 in 40 mM bicine, pH 8.0, 10 μM EDTA. Plots of $v/[E]$ vs $[Na_2SO_4]$ were fit to eq 5, which describes a saturation binding isotherm in which the *y* intercept may be nonzero (v_0). The parameter v_{max} represents the maximal value of $v/[E]$, and K_d is the apparent dissociation constant for sulfate ion.

$$v_{obs} = v_0 + \frac{v_{max}[SO_4^{2-}]}{K_d + [SO_4^{2-}]} \quad (5)$$

Crystallographic Methods. Single crystals of W39V/G41A were grown over several days in 0.15 M Na/KH_2PO_4 at pH 7.5 and 10 mg/mL protein at 22 °C using hanging drop vapor diffusion. The best crystal size was achieved when the initial drop was diluted 1:1:1 with protein/well solution/storage buffer (20 mM TrisCl, 10 μM EDTA, pH 8.0) to slow initial nucleation. Crystals were soaked in artificial mother liquor plus 30% glucose and 0.5 M $NaHCO_3$ for 30 s prior to flash cooling in liquid nitrogen. Similarly, single crystals of W39V/G41A/P48S/A49P were grown in 0.30 M Na/KH_2PO_4 at pH 7.5 and 12 mg/mL protein at 22 °C using hanging drop vapor diffusion and cryoprotected using artificial mother liquor plus 30% glucose. Single, tetragonal crystals of P48S/A49P HICA were grown over 4−6 weeks in 1.5 M $(NH_4)_2SO_4$ and 5% DMSO at pH 6.5 from 13 mg/mL protein. Crystals were cryoprotected in artificial mother liquor plus 30% glucose. Crystals were flash cooled in liquid nitrogen.

Data collection for all structures was carried out on an Oxford Diffraction Gemini R system using a PX Ultra Enhance Cu Kα source (1.54 Å) and a Ruby CCD detector. Data was processed using CrysAlisPro[40] and SCALA,[41] and an initial molecular replacement solution was obtained by using a search model derived from a single dimer of wild-type HICA (PDB 2A8D) in Phaser.[42] The initial solution was subjected to multiple rounds of refinement using Refmac5[43] and model-building in Coot.[44,45] Final refinement incorporated TLS[46] with one TLS group per protein chain. Simulated annealing omit maps ($2F_o - F_c$ and $F_o - F_c$ difference Fourier maps) were used to verify the correctness of the models; superposition of P48S/A49P chains and wild-type HICA (2A8D) was done using the program Superpose in the CCP4 suite of programs. Data collection and refinement statistics are reported in Table 1.

Absorption Spectroscopy of Co(II)-Substituted HICA. UV−visible spectra of Co(II)-substituted P48S/A49P HICA were measured at 25.0 °C using an Ocean Optics USB-4000 spectrometer and a 1 cm path length, 40 μL microcell (Starna). The pH of the solution was controlled with 100 mM concentrations of MES (pH 6.51), MOPS (pH 6.92−7.53), HEPES (pH 7.75−8.00), Bicine (pH 8.25−9.00), or CHES (pH 9.25−10.50). Enzyme concentrations varied between 300 and 850 nM.

RESULTS

Overexpression, Purification, and Quantification Were Consistent with Wild-Type Enzyme. All variants eluted from the gel exclusion column at a solvent volume corresponding to an apparent molecular weight of ≈100 kDa, equivalent to the wild-type tetramer. Co(II)-substituted P48S/A49P eluted from the hydrophobic interaction column with a pale green color, which shifted to a deep blue color after gel exclusion chromatography (also consistent with the Co-substituted wild-type). ICP-OES analysis for Zn (213.856 nm) and Co (228.616 nm) in the Co(II)-substituted P48S/A49P HICA variant yielded 327 μM Co and 34 μM Zn, representing 91% substitution of Co. Spectroscopic data was based on a Co concentration of 327 μM.

Steady-State Kinetics Vary in Rate Cooperativity by Variant. The pH−rate profiles of k_{cat}/K_m for the W39V/G41A, P48S/A49P, and W39V/G41A/P48S/A49P variants of HICA vary in their pH−rate cooperativity (Figure 2) compared to

DOI: 10.1021/bi501116e
Biochemistry 2015, 54, 598−611

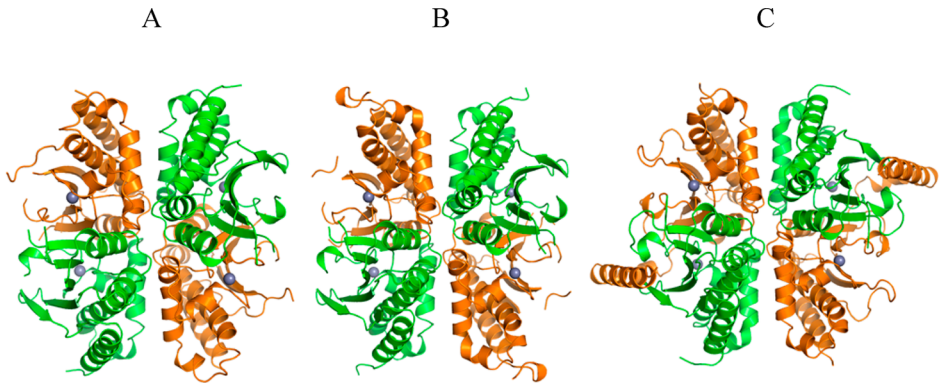

Figure 3. Subunit organization of (A) HICA-W39V/G41A, (B) HICA-W39V/G41A/P48S/A49P, (C) HICA-P48S/A49P. Chains A and B of the allosteric dimer are colored green and orange. Active site zinc ions are depicted as gray spheres. The allosteric dimers (A chain + B chain) are associated with form a biological tetramer through a tetramerization interface, which is vertical in these figures. The dimerization interface is horizontal.

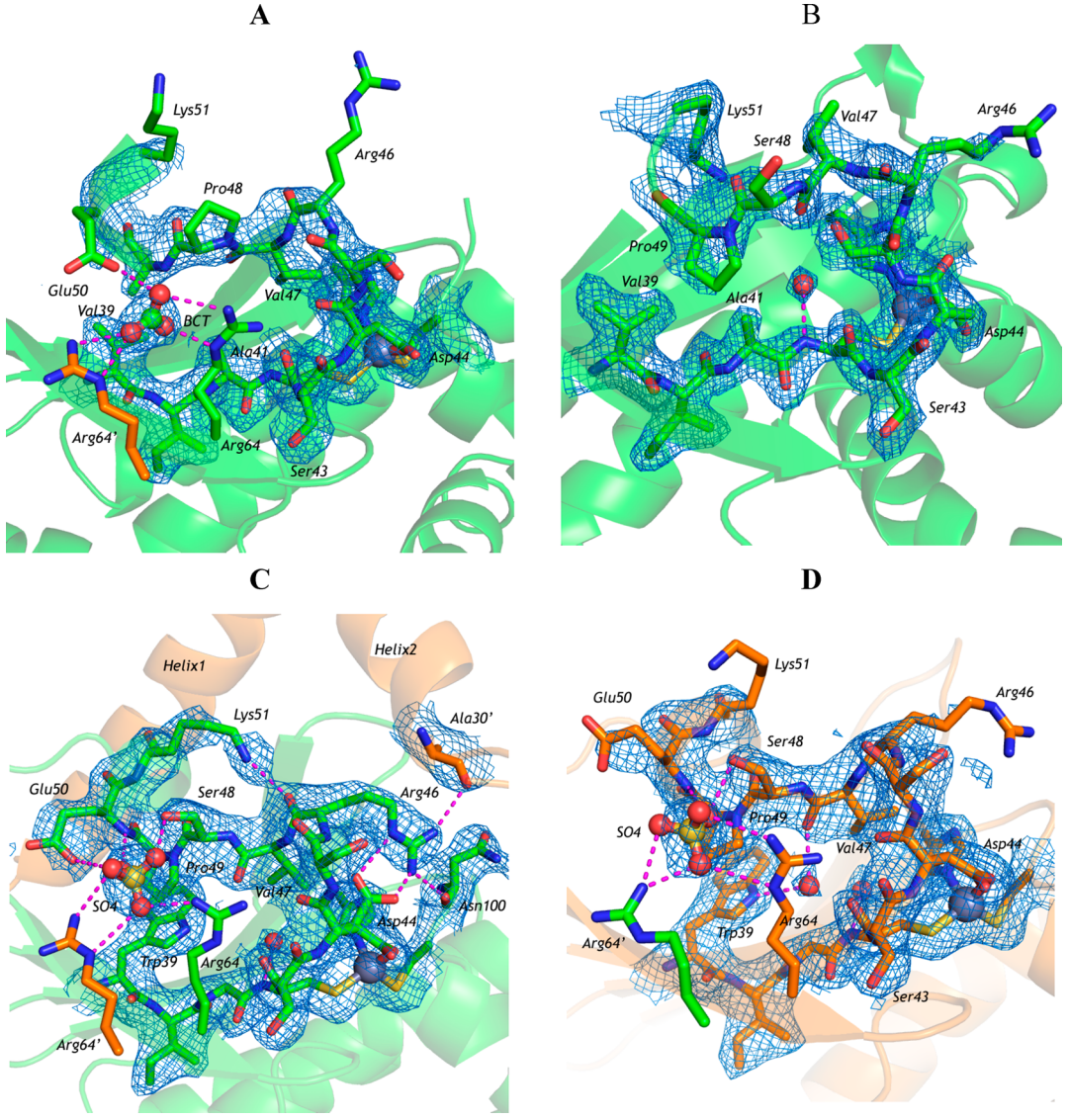

Figure 4. Activation loop positions of HICA variants (A) W39V/G41A, (B) W39V/G41A/P48S/A49P, (C) P48S/A49P chain A, and (D) P48S/A49P chain B. $2F_o - F_c$ maps of residues 39−51, including zinc ion and ligands (Cys 42, Asp 44, His98, Cys101), contoured at 1.0σ (A, B, D) or 0.7σ (C). Anions and water molecules in these sites are also contoured at the same level. Residues 39−51, Arg64, and metal ligands are depicted as sticks, anions, as ball and stick, water molecules, as red spheres, and zinc ions, as gray spheres. Selected hydrogen-bonding interactions are depicted as dashed magenta lines.

DOI: 10.1021/bi501116e
Biochemistry 2015, 54, 598−611

that of wild-type HICA. The pH−rate profile of k_{cat}/K_m W39V/G41A shows a two-proton dependence that suggests that two H^+ ions must be lost to form the active form of the enzyme, unlike that of the wild-type enzyme, which fit to a four-proton dependence.[17] The pH−rate profile of k_{cat}/K_m of P48S/A49P and W39V/G41A/P48S/A49P HICA shows no cooperativity in proton loss and fit well to a single-proton dependence. Maximal k_{cat}/K_m values of the W39V/G41A and P48S/A49P variants are higher than that of the wild-type enzyme. Maximal values for the W39V/G41A variant of k_{cat}/K_m =16 ± 2 μM^{-1} s^{-1} and for the P48S/A49P variant of k_{cat}/K_m = 17 ± 3 μM^{-1} s^{-1} are 380 and 405% of wild-type maximal values, respectively. The apparent pK_a values of the k_{cat}/K_m profiles for W39V/G41A and P48S/A49P variants (8.32 ± 0.04 and 8.3 ± 0.1, respectively) are also higher than the wild type enzyme (pK_a = 7.74 ± 0.04) but are indistinguishible from each other. The pH−rate profile for the W39V/G41A/P48S/A49P variant did not show an apparent pK_a transition in pH range 6−9, but rather it showed a linear dependence on pH that did not plateau within the experimental pH range.

Variations in the pH dependence of k_{cat} follow a similar pattern. The pH profiles of the wild-type enzyme and W39V/G41A show different degrees of cooperativity (four- and two-proton dependencies, respectively), whereas the proline shift variant P48S/A49P shows a lack of cooperativity (a single-proton dependence) in the pH profile of k_{cat}. The apparent k_{cat} of the quad variant W39V/G41A/P48S/A49P does not plateau in the pH range 6−9.

Structure of W39V/G41A Shows Bicarbonate Ion Trapped in the Escort Site. HICA-W39V/G41A (PDB 4WAK) is nearly identical in overall structure to wild-type HICA. The asymmetric unit contains two chains, which, with crystal symmetry, describes a dimer of dimers identical in quaternary structure to wild-type HICA (Figure 3A). A tight dimerization interface extends the central β-sheet across two chains to define the allosteric dimer and that is in close proximity to the active site zinc ion. A tetramerization interface is orthogonal to the dimerization interface and provides for the interaction and association of the consistently observed four chains. This interface is characterized by a cluster of basic amino acid side chains: Arg160, Lys165, and Arg198 from one dimer and Arg 124 from the neighboring dimer. Similar to wild-type HICA, this tetramerization interface shows two strong electron density peaks in the variant; these electron density peaks were spherical in the wild-type HICA and were interpreted as sulfate ions. In HICA-W39V/G41A, which is soaked with 500 mM $NaHCO_3$, the disc-like electron density has been interpreted as HCO_3^- (Figure 4A) based on the absence of polyatomic anion electron density in the structure of the unsoaked enzyme, the shape of the electron density, and the B-factor.

However, the structure of HICA-W39V/G41A differs from the wild-type enzyme in several regions: there is no discernible electron density for the N-terminal α-helices (residues 1−33); presumably, these residues are disordered in the crystal. Electron density is also weak or missing for two surface loops (residues 53−57 in both chains and 183−184 in chain B) that are often disordered in other HICA structures. In the activation loop, Val47 has swung from the exterior of the protein directly into the allosteric site. Although the active sites of all chains are identical to the T-state of wild-type HICA, where Asp44 is ligated into the first coordination sphere of the zinc ion (Figure 4A), crystals of HICA-W39V/G41A soaked in 500 mM $NaHCO_3$ show no additional electron density that can be interpreted as HCO_3^- in the allosteric site, and no previously observed hydrogen-bond-donating side chains are oriented toward the space (e.g., Trp39, Ser45, Tyr181, or the backbone carbonyl of Val47). Instead, HCO_3^- is trapped in the escort site.

Structure of the W39V/G41A/P48S/A49P Variant Reveals Displaced Activation Loop Backbone. HICA-W39V/G41A/P48S/A49P (PDB 4WAM) is also identical in quaternary structure to wild-type HICA (Figure 3B). There is again no discernible electron density for the N-terminal α-helices (residues 1−33), and the surface loops including residues 53−57 in both chains and residues 182−191 in the A chain have weak or no electron density, as with the HICA-W39V/G41A variant. In the active site, Asp44 occupies a ligand position around the zinc ion and is making hydrogen bonds to a water molecule (Figure 4B). In the activation loop, residue Ser45 is flipped into the allosteric pocket but is not making polar contacts to anything in the pocket; Arg46 is weakly described by electron density, with no clear interaction with anything, and Val47 is in a midflip position, neither in nor out of the allosteric pocket, whereas no side chain density is visible for Ser48. There is one water molecule in the allosteric pocket itself, within hydrogen-bonding distance of the amide nitrogen of Cys42.

Structure of the P48S/A49P Variant Reveals Two Different Chain Conformations. The overall protein fold of P48S/A49P HICA (PDB 4WAJ) is also nearly identical to that of wild-type HICA, with a C_α rmsd of 0.97 Å (Figure 3). However, the structure of P48S/A49P HICA differs markedly from the wild-type enzyme in several places. In chain A, no visible density is seen for residues 1−33 (helix 1 and 2). There is a significant deviation of 1−4 Å rmsd around the activation loop of 44−51, as well as in helix 3, and similar deviations are present in an additional area beginning at residue 181 and continuing through the first half of the twisted β-strand to residue 195. In P48S/A49P HICA chain A only, the side chain of Arg46 is well-described by the electron density, in a key central position between Ala30′ and Asp44. Compared to the B-chain, the electron density for Asp44 density in the A chain is not completely described by a single position and seems to be distorted slightly toward Arg46. Chain A is consistent with both the T-state, where Asp44 is bound to the active site metal ion, and R-state, where Arg46 (stabilized by Ala30′) is in a position to interact with a detached Asp44. Compared to wild-type HICA, there are two more differences: the side chain of Ser45 has swung away from the allosteric site toward bulk solvent, and Arg46 makes additional contacts to the backbone carbonyl oxygens of Asp100, as well as Asp44 and Ala30′ (Figure 4C).

Unlike any HICA structure reported so far, there are differences between HICA-P48S/A49P A and B chains. Chain B also shows the side chain of Val47 flipped completely into the allosteric pocket, but the rest of the activation loop and, indeed, the active site conformation are identical to the T-state of wild-type HICA: Asp44 is ligated into the first coordination sphere of the zinc ion, there is little discernible density present for Arg46, and Ser45 remains flipped out to bulk solvent (Figure 4D.) Notably, in the B chain of P48S/A49P HICA, there is clear density for residues 1−35 of the N-terminus, comprising a helix−loop−helix and a long loop connecting them to the rest of the monomer. These helices, as with the wild-type structure, are dimer-exchanged, where Ala30 of the long connecting loop contributes to the hydrogen-bonding network of the active site

DOI: 10.1021/bi501116e
Biochemistry 2015, 54, 598−611

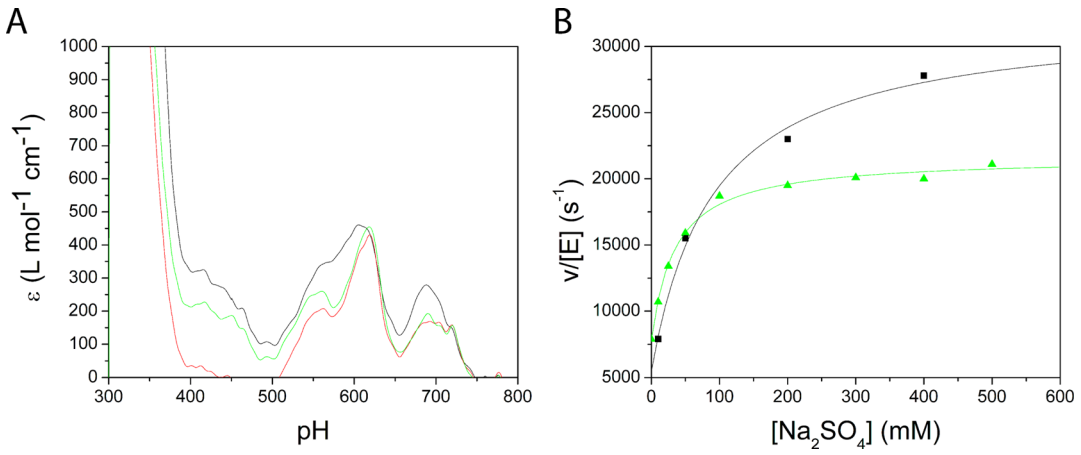

Figure 5. Influence of anions on P48S/A49P HICA. (A) Absorption spectra of cobalt-substituted P48S/A49P HICA at pH 7.00 (black line), pH 8.00 (red line), and pH 8.00 and 0.1 M bicarbonate (green line). (B) Sulfate dependence of CO_2 hydration activity of wild-type (black squares) and P48S/A49P HICA (green triangles) in 40 mM bicine, pH 8.50, 1 μM EDTA, 8.0 mM CO_2, 25 °C. Data were fit to eq 5, with ν_{max} = 26.8 ± 2.3 ms^{-1} and K_d = 91 ± 39 mM (wild-type HICA) and ν_{max} = 13.9 ± 0.4 ms^{-1} and K_d = 35 ± 4 mM (P48S/A49P HICA).

of the other chain. Compared to wild-type HICA, the C_α rmsd for N-terminal residues 20−28 is substantial, between 3.5 and 4.8 Å, with P48S/A49P HICA packing the N-terminal helices significantly closer to the adjacent protein chain. In this area, residue Tyr 181 of the dimer has flipped out of the wild-type nonallosteric binding site and is contributing to the hydrophobic packing with the N-terminal helices. Likewise, Lys51 has discernible density in that new hydrophobic core and donates a hydrogen bond to the carbonyl of Arg46. The long connecting loop between helix 1 and helix 2 has a significant C_α rmsd of 5.2 and 5.9 Å for residues 31 and 32, respectively, compared to wild-type because, in the variant structure, these residues have undergone a helix-to-coil transition, positioning them (and catalytic residue Gln33′) significantly closer to the neighboring chain active site.

Spectroscopic Characterization of Co(II)-Substituted P48S/A49P HICA Confirms the Variant Is Unresponsive to Inhibitory Bicarbonate. The absorption spectrum (Figure 5A) of Co(II)-substituted P48S/A49P HICA at pH 8.0 has visible absorption bands nearly identical to the wild-type Co-HICA spectrum[16] with maxima at 560 nm (ε = 210 M^{-1} cm^{-1}), 620 nm (ε = 450 M^{-1} cm^{-1}), and 703 nm (ε = 156 M^{-1} cm^{-1}). Also similar to wild-type is that, when pH is lowered to 7.00, the molar absorptivity of P48S/A49P HICA in the visible region markedly increases (Figure 5A). Unlike wild-type Co-HICA, there is no significant red shift of the 560 nm band at low pH, reflecting subtle changes to the metal coordination sphere. Likewise, the absorption spectrum at high pH also does not visibly change to that characteristic of the T-state as a result of the addition of 100 mM sodium bicarbonate.

Sulfate Dependence of HICA-P48S/A49P. Both wild-type HICA and HICA-P48S/A49P are activated by sulfate ion at pH 8.0 (Figure 5B), a phenomenon that has never been fully rationalized. However, the apparent K_d for sulfate is significantly lower (35 ± 4 mm) for the proline shift variant compared to the wild-type enzyme (91 ± 39 mM).

DISCUSSION

We identified four residues in the HICA activation loop that differed from the equivalent residues in the nonallosteric β-CA structure of PSCA. Previously reported single variants of Gly41[23] and Trp39[24] were insufficient to revert HICA to a nonallosteric enzyme, so we constructed double variants of these residues, a proline shift variant and complete mutation of all four residues (W39V, G41A, P48S, and A49P). The quad variant W39V/G41A/P48S/A49P disrupted the position of the activation loop and kinetic turnover of the variant so significantly (it does not resemble any previously studied HICA vasriant or PSCA) that we conclude there must be additional, unknown factors in PSCA beyond these four residues that account for its kinetic behavior. The double variants, on the other hand, were apparently conservative enough to maintain critical structural features while successfully altering the allostery of HICA.

Kinetics of Allosterically Altered Enzymes. The overall catalytic turnover of W39V/G41A and P48S/A49P variants of HICA is maximal at pH > 8.0 (Figure 2A), suggesting that the metal-hydroxide form of the enzyme is the active species, consistent with wild-type HICA. The two-proton cooperative dependence of k_{cat} has been interpreted as the cooperative deprotonation of a water molecule to hydroxide in the two active sites of the tightly associated dimer.[17] The similar limiting slope of the W39V/G41A variant, then, suggests that the cooperativity of catalysis remains intact. The loss of two-proton dependence in the slope of the P48S/A49P variant of HICA, visible in the shallow slope of the line, more obviously completely disrupts the cooperativity of the variant in maximum catalytic turnover: the two active sites are kinetically independent.

Both the W39V/G41A and P48S/A49P variants show disrupted allostery for the specificity constant pH−rate profiles (Figure 2B). The wild-type k_{cat}/K_m pH−rate profile (Figure 2B) describes a cooperative four-proton loss with an apparent pK_a value of 7.74 ± 0.04, which is most likely due to a cooperative loss of two protons from each of the two chains in the allosteric dimer.[17] The substitution of W39V/G41A substantially changes the pH−rate cooperativity of the enzyme, from a four- to a two-proton dependence with an apparent pK_a value of 8.2 ± 0.1. This disrupted protonation dependence might be a result of decoupling the cooperativity between the allosteric dimer active sites, retaining two deprotonation events for activation of each individual subunit, or it might also be explained by the loss of one deprotonation event on each of the two chains of the allosteric dimer, leaving two cooperative, one-

DOI: 10.1021/bi501116e
Biochemistry 2015, 54, 598−611

proton events for activation of the enzyme. Considering together the disrupted k_{cat}/K_m kinetics with the unchanged pH−rate profiles of k_{cat}, we conclude that at least some of the cooperativity between subunits is intact for the W39V/G41A variant.

The P48S/A49P variant of HICA completely disrupts the cooperativity for the k_{cat}/K_m kinetics: the pH−rate profile for this variant is consistent with the ionization of a single group generating the active form of the enzyme. The single-proton dependence of k_{cat}/K_m, consistent with identical pH−rate dependence of k_{cat} kinetics, suggests that the individual active sites have been decoupled entirely: both the cooperativity in active site turnover and the additional deprotonation associated with transition to the R-state. The apparent pK_a value for that remaining group in the k_{cat}/K_m curve is 8.3 ± 0.4, which is consistent with a zinc-bound water molecule but slightly higher than the value of 7.74 ± 0.04 for the cooperative four-proton dependent wild-type enzyme.

The higher apparent pK_a value observed in P48S/A49P variant of HICA can be interpreted within the hypothesis that the cooperative apparent pK_a in the wild-type enzyme is due to two crossed two-proton ionizations at least 0.5 pH units apart that average to a value of 7.74.[17] The decoupling of these pK_a values would leave a zinc−water pK_a value of >8.2 or <7.2. Since k_{cat}/K_m in the zinc-hydroxide mechanism should track with the metal-bound water molecule, this result suggests that the zinc-bound water molecule in the P48S/A49P variant, and perhaps in the wild-type enzyme as well, has an intrinsic pK_a near 8.3. The more acidic pK_a, <7.2, remains to be identified, but it is absent in the P48S/A49P variant.

The quadruple variant W39V/G41A/P48S/A49P revealed anomalous pH−rate kinetics: the pH profile of k_{cat}/K_m at steady state did not plateau above pH 8.0; rather, the profile is approximately log−linear with a slope of +1 in the k_{cat}/K_m profile, suggesting a loss of cooperativity and the possibility that the pK_a may have been shifted above the range of our experiment. We interpret this as the absence of stabilizing influence, provided in the PSCA structure, for which we have not accounted.

The variants reported here have maximal k_{cat}/K_m values as much as 400% that of the wild-type enzyme, a result that is consistent with the stabilization of the R-state of the enzyme relative to the T-state. Previously reported variants of HICA have been observed to have maximal k_{cat} or k_{cat}/K_m of 50−200% of wild-type enzyme, consistent with the interpretation that all of our variants reported here may have slightly increased the fraction of the enzyme that is active at any given pH.

Structure of Allosteric Variants of HICA. Given the partially or completely disrupted allostery in our kinetically active variants, we hypothesized that the structures would be consistent with our model of allosteric communication. What we found in the comparison of wild-type to W39V/G41A and P48S/A49P structures suggests a greater role for the activation loop in general and a decreased importance of Val47 in particular. An analysis of all three structures additionally reveals a new role for the N-terminal dimer-exchanged helices in intersubunit communication and increased importance of the escort site at the top of the activation loop.

The structure of the W39V/G41A partially allosteric variant reveals a T-state at the metal active site (Figure 4A), a structure that is nearly identical to most deposited structures of HICA. Arg46, at one end of the activation loop, has little density to describe it, but Asp44 is clearly ligated to the metal. Unusually, the activation loop has flipped Val47 into the allosteric site, a position associated with nonallosteric β-CAs or the proposed R-state for HICA, even though the active site remains in a T-state. Val47 continues to occupy the allosteric pocket even when the crystal is soaked with a high concentration of bicarbonate, suggesting that the position of Val47 may not be determinant for the active site state as previously supposed. We do observe bicarbonate coordinated at the top end of the activation loop, in the escort site of the structure (the entrance to the allosteric pocket), which is consistent with the G41A single variant structure.[23]

We have noticed significant flexibility in the activation loop in other HICA variants, but the standing hypothesis had identified Val47 as the linchpin residue for displacing the bicarbonate from the allosteric pocket and translated that absence of inhibitor through the backbone position of the activation loop to Asp44. The position of Val47 in the W39V/G41A structure is inconsistent with Val47 in a driving role. The coordination of bicarbonate in the escort site in this semicooperative variant is intriguing, however, suggesting that bicarbonate's position in the allosteric site (the middle of the activation loop) is less important than whether it is able to bind or pass through the escort site (the top of the activation loop).

The structure of P48S/A49P is the first kinetically active variant of HICA to crystallize in a state where Arg64 of the activation loop is well-defined and a key contact between Asp44 and Ala30′ of the dimer-exchanged capping loop is seen. The bidentate contact between Arg64 and Asp44 in chain A stabilizes Asp44 rotated away from the catalytic zinc, a position that would allow a water molecule to take the fourth ligand position and Asp44 to coordinate CO_2 substrate. The Arg46 contact with Ala30′ of the capping loop is significant due to the role of Gln33′ in bicarbonate coordination in catalysis. In the P48S/A49P structure, the Gln33′ side chain is disordered, but there is also no product in the active site to coordinate; the backbone position of Gln33′ has been rotated directly toward the active site, however, and is primed to coordinate product.

The complete disruption of cooperativity in the P48S/A49P variant is supported by observation that only one of the two protein chains in the allosteric dimer appears to have clear electron density for Arg46 in a position to allow interaction with an Asp44 residue detached from the metal ion. Chain B (Figure 4D), with Asp44 as a ligand to zinc, serves as an internal control: it displays all of the common features seen in T-state HICA structures. There is no obvious water ligand to the metal ion, Arg46 shows little to no density in the side chain (suggesting it is disordered), and there is strong, localized density for Asp44 bound to zinc. Unusually, Ser45 is flipped out of the allosteric site in both chains of P48S/A49P, as is Tyr181 (both of which donate hydrogen bonds to allosteric bicarbonate in the wild-type bicarbonate-bound structure). Like the W39V/G41A variant, Val47 in the middle of the activation loop is flipped into the allosteric site in both chains. Since the two active sites in the P48S/A49P variant are in different conformations, but Val47 position is conserved, this again argues against the role of Val47 as a key residue in allosteric communication; it may simply be part of a rather flexible loop in the absence of other stabilizing or steric factors, such as allosteric bicarbonate binding.

Interestingly, for chain B only of P48S/A49P, the N-terminus of the chain is completely described with good density throughout the backbone, packing tightly against the amphipathic C-terminus of helix 3 of the neighboring chain.

DOI: 10.1021/bi501116e
Biochemistry 2015, 54, 598−611

The end of helix 2 contributes a hydrogen-bond contact from Ala30′ backbone carbonyl to Arg46 of chain A in the active site (Figure 3C) and may be a much better candidate for a pathway of allosteric communication than Val47.

Al alternative allosteric communication pathway is suggested by an analysis of the specific impact of the proline shift: The P48S/A49P mutations are distal to the active site, only partially associated with the allosteric pocket, and indeed are at the far end of the activation loop. We were surprised to find that the proline residues at the dimerization interface describe a binding pocket in the escort site that is well-suited for a tetrahedral ion (Figure 6). We observe binding of sulfate at this dimerization

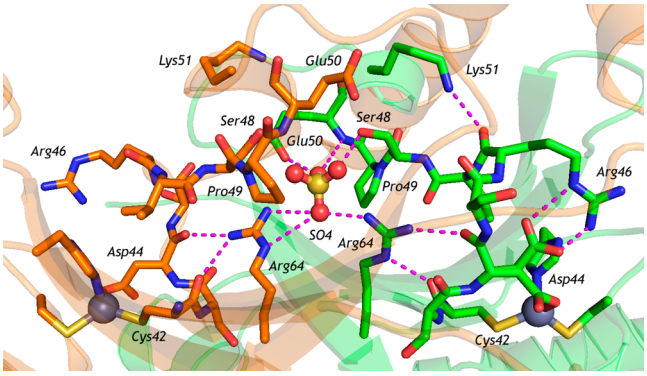

Figure 6. Asymmetric hydrogen-bonding network around the anion binding (escort) site and active sites of HICA-P48S/A49P. Key residues of chain A (green) and chain B (orange) are depicted as sticks. Sulfate is depicted as ball and stick. Zinc ions are gray spheres. Selected hydrogen-bonding interactions are depicted by magenta dashes.

site in both the wild-type and P48S/A49P HICA structures, rather than a bicarbonate ion observed in several allosteric site variants of HICA.[23] Indeed, we were not able to see characteristic electron density for bicarbonate in the escort site in P48S/A49P variant even when we soaked the crystals with high concentrations of bicarbonate. This suggests that the P48S/A49P double variant is enough to optimize the escort site for a tetrahedral anion and remove the ability for planar bicarbonate to compete.

Position 49 defines the beginning of helix 3 in the structure, but the proline substitution in P48S/A49P significantly alters the angle and position of the helix compared to the wild-type alanine: the shift in rmsd position results in the helix crowding closer to the sulfate ion in the escort site. This tilt may also be influenced by the mutation at position 48 to serine (a mimic for Cys in PSCA), which is oriented toward the pocket and is close enough to contribute to a hydrogen-bond contact. Otherwise, the sulfate ion in the P48S/A49P structure is in a location that allows it to make the same hydrogen-bond contacts to residues Arg64 (from both chains) and one Glu50 residue from helix3 of the A chain, a contact that has also been observed in the W39V/G41A and wild-type HICA escort sites. Helix 3 in the P48S/A49P structure is more tightly associated with the escort site than the wild-type HICA soaked with bicarbonate (which has no ion in the escort site due to bicarbonate entering the allosteric pocket). If the Val47 position (flipped in in the R-state, flipped out when bicarbonate is bound) is indeed a byproduct rather than the driver of allosteric communication, then, potentially, the shift in helix3 position might be the primary structural change in the communication pathway.

We observed a number of variations in contacts to helix 3 in the activation loop of the A and B chains that are associated indirectly with the R-state to T-state transition in HICA (Figure 7). First, Lys51 in helix 3, disordered in the T-state chain B as

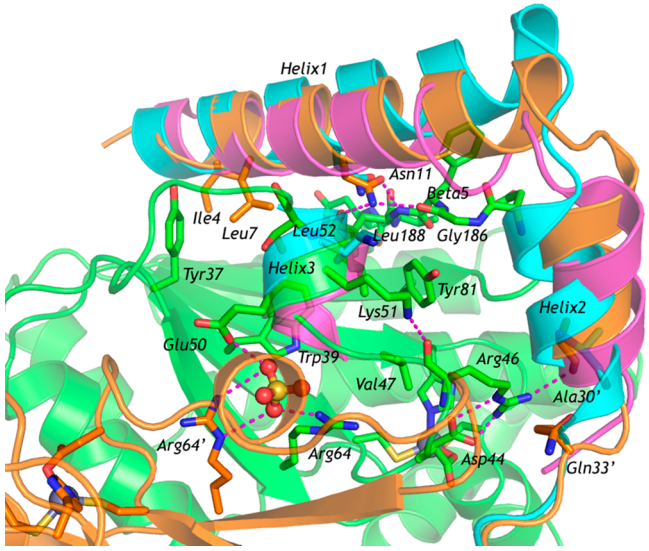

Figure 7. Intersubunit contacts in the allosteric dimer of HICA-P48S/A49P chain A are depicted as orange cartoons/sticks; chain B is depicted as green cartoons/sticks. Key residues are depicted as sticks. The allosteric site is directly behind helix 3. Sulfate ion occupies the escort site and is depicted as ball and stick. Zinc ion is depicted as a gray sphere. Selected hydrogen-bonding interactions are depicted as magenta dashes. Cyan cartoons and sticks represent a superposition of the wild-type HICA allosteric dimer on the HICA-P48S/A49P structure. Wild-type residues 1−37, comprising helix 1 and helix 2, and residues 50−53, comprising helix 3, are depicted. Magenta cartoons represent a superposition of PSCA on the HICA-P48S/A49P structure. PSCA resicues 119−151, comprising helix 1 and helix 2, and residues 166−171, comprising helix 3, are shown.

well as wild-type HICA structures, is well-described in the P48S/A49P chain A making a hydrogen-bond contact to the backbone carbonyl of Arg46. The Lys51 hydrogen bond to Arg46 is enabled by the tilt and rotation of helix3, and the contact stabilizes the entire activation loop in a position that not only orients the key Arg46 side chain but also flips Val47 into the allosteric pocket (Figure 4C, 6). Perhaps, as a result of the stable hydrophobic character of the allosteric pocket, Tyr181 (which donates a hydrogen bond to bicarbonate ion in an occupied allosteric site) is repositioned to pack in a newly defined hydrophobic core between the top of the activation loop (Leu52 and Thr53 from helix 3) and the structured N-terminus from the chain B. This interaction is additionally stabilized by 3 polar contacts between residue Asp11′ from the helix 1 to the backbones of helix 3 (Leu52) and β5 (Leu188 and Gly186); there are additional hydrophobic intrahelical stabilizing contacts as well (Figure 7). The newly formed hydrophobic core between the activation loop and the N-terminal helices appears to be well-stabilized in this structure, apparently as a result of a number of small conformational changes that correctly position the activation loop.

The N-terminal H1-L1-H2-L2 segments comprise residues 1−35 of HICA and are often disordered in structures of HICA variants, presumably due to high mobility and multiple conformations of these residues. Notably, one structure in which the N-termini were visible in all chains is that of wild-

DOI: 10.1021/bi501116e
Biochemistry 2015, 54, 598−611

type HICA, which allows us to compare it to the single visible N-terminus in chain B P48S/A49P HICA, which is dimer-exchanged to associate with R-state chain A. A striking difference in the two structures, despite the visible N-terminal helices, is located in the second loop at the base of helix 2, which caps the active site of the neighboring chain in the allosteric dimer. In the P48S/A49P variant, this capping loop makes a hydrogen-bond contact from the backbone of Ala30′ (chain B) to the key residue of Arg46 (chain A, Figure 6) and simultaneously rotates Gln33′ toward the active site, in preparation for coordinating CO_2 and HCO_3^- in catalysis.[33] In the wild-type structure, Gln33′ is rotated away from the active site, with the backbone oriented in such a way that no rotation of chi-angles can bring the side chain into proper position for catalysis. Clearly, the structured appearance of the wild-type N-terminal helices alone was not enough to stabilize the catalytic residues in an R-state for the crystal.

The difference in catalytic residue backbone position may be explained by a helix-to-coil conformational change: in the P48S/A49P structure, the last turn of helix 2 of chain B (including Ala30′) has unwound into a coil. The new coil is well-described by electron density at the backbone, allowing the Ala30′−Arg46 contact and rotating the backbone of Gln33 nearly 180° from the wild-type structure (Figure 7). The Gln33′ side chain is still largely disordered in the P48S/A49P structure (consistent with the absence of CO_2 and HCO_3^- in the active site), but it is now in close proximity to Arg46, Asp44, and Tyr83, which define the substrate binding pocket.

Superposition of the wild-type enzyme (PDB 2A8D) and HICA-P48S/A49P showed the N-terminus of P48S/A49P (including residues 30′−33′) along with the allosteric loop and helix 3 (residues 50−53) to have average C_α rmsd > 2.0 Å in both chains compared to wild-type. In wild-type HICA, the principal axis of helix 1 is rotated about 6.7° around the N-terminus, away from β5 compared to HICA-P48S/A49P. (The anchor of the helix rotation appears to be around a cluster of residues formed by Tyr37, Ile4, and Leu 7. Tyr37 appears to anchor helix 1 to β1 in HICA.) This helix rotation results in a shift of Asn11, which makes polar contacts with β5 and helix 3, by 1.5 Å. In HICA-P48S/A49P, Asn11 makes three hydrogen bonds: to the carbonyl oxygen atoms of Gly186 on β5 and Leu52 on helix 3 and the amide nitrogen of Leu188 on β5. In the wild-type enzyme, the contact with Gly186 is lost. The rotation of helix 1 away from β5 in the wild-type enzyme results in a repositioning of helix 3 and Lys51 by about 1.5 Å relative to HICA-P48S/A49P. The repositioning of Lys51 in the wild-type enzyme breaks the Lys51−Arg46 carbonyl backbone interaction that helps to stabilize the orientation of Arg46 to interact with Asp44 and Ala30′. The difference in position of the N-terminal helices in the wild-type and P48S/A49P variant reaches a maximum of 6 Å at loop 1 between helix 1 and 2: in the P48S/A49P variant, this helix shift repositions and twists helix 2, moving the carbonyl oxygen of Ala30′ some 5.2 Å, where it can can interact with Arg46 and lock it into position in the active site. This helix reorientation also brings Glu33′ closer to the active site of the enzyme.

The nonallosteric PSCA has a conformation for helices 1−3 that closely parallels that of the R-state monomer of HICA-P48S/A49P (Figure 7). Helix 1 of PSCA deviates from the HICA-P48S/A49P by no more than 1.5 Å, displaced slightly closer to β5 than in HICA-P48S/A49P. Helix 2 of PSCA is tilted outward at its N-terminus, but the C-terminus is in nearly the identical location as in HICA-P48S/A49P. In PSCA, Arg164 (the equivalent of Arg46 in HICA) interacts with the carbonyl oxygen of Leu147′ instead of Ala148′ (which is the equivalent of Ala30′ in HICA). Helix 3 is in a nearly identical position is both PSCA and HICA-P48S/A49P. However, in PSCA, there is no equivalent of Lys51: in PSCA, this residue is a histidine residue (His169), which appears to be solvent-exposed.

The Anion Requirement of HICA. One of the consequences of the displacement of helix 3 toward the active site in HICA-P48S/A49P relative to the wild-type enzyme is the creation of an efficient coordination environment for an anion in the escort site, in particular, Glu50, which, in concert with Arg64′ and Arg64, stabilizes the activation loop in the R-state conformation. HICA requires unusually high sulfate concentrations (250 mM) for maximum activity. We hypothesize that this sulfate requirement, as well as the cooperative product inhibition by bicarbonate, could be structurally explained by anion competition in the escort site: the site in the dimer interface that leads to either chain's allosteric pocket and is at the top of either chain's activation loop. It was originally hypothesized that the presence of high concentrations of sulfate or phosphate competed with bicarbonate for escort site binding, preventing passage of bicarbonate from bulk solvent to either allosteric site.[23] The first functionally and structurally nonallosteric HICA variant presented us with the opportunity to test this hypothesis.

To explore whether bicarbonate is still capable of inhibiting P48S/A49P HICA, we monitored the established spectroscopic transitions between the T- and R-states at the metal sites as a function of pH and in the presence of 100 mM bicarbonate. Cobalt-substituted P48S/A49P HICA at high pH (Figure 4A) reveals absorption spectra similar to wild-type and retains the peaks and molar absorptivities in the visible region associated with four-coordinate Co(II) sphere d−d transitions (peaks at 560, 620, and 700 nm and >200 L mol^{-1} cm^{-1} absorptivities). The lower pH spectra reveal an expected increase in absorptivities with increased proton concentration; however, the red shift of the 560 nm peak to 580 nm, consistent with the cooperative pK_a of wild-type HICA and presumed quantitative coordination of metal by Asp44, is noticeably absent. We theorized that the 560 nm peak shift might have represented the ligand binding to Asp44 in the T-state, a tight association that might have shifted the pseudotetrahedral coordination of the metal more than a free-associated water or hydroxide ion would. In the P48S/A49P structure, we see both a T- and R-state position for Asp44, so the expected absorptivity change, and unexpected absence of peak shift, implies that the equilibrium between T- and R-states has been shifted enough that Asp44 no longer ligates the metal so tightly as to distort the pseudotetrahedral coordination sphere.

When 100 mM bicarbonate is added to the bulk solution at high pH (pH 8.0), again, no significant change in the 620 or 700 nm peak is observed, and only a small increase in absorptivity (from 210 to 260 L mol^{-1} cm^{-1}) is observed at the 560 nm peak. This concentration of bicarbonate is sufficient to trip wild-type Co-HICA from the R-state to the T-state at pH 8.0, as observed by shifts in the 620 and 700 nm peaks. That this concentration of bicarbonate ion is not capable of inducing a similar T → R transition for the Co(II) derivative of HICA-P48S/A49P is further confirmation of the disruption of cooperativity.

Even with no bicarbonate inhibition in the P48S/A49P variant, we observed a structural anion in the escort site that

DOI: 10.1021/bi501116e
Biochemistry 2015, 54, 598−611

seemed to be optimized for a tetrahedral anion. Our initial hypothesis had postulated that planar and tetrahedral anions compete for the escort site and explained the high sulfate requirements of HICA in kinetic studies (to outcompete bicarbonate). To explore whether the sulfate anion present in our kinetic studies is still required in the P48S/A49P variant, we performed a kinetic study of CO_2 hydration kinetics with varying sodium sulfate concentrations (Figure 4B). We found that the CO_2 hydration activity of P48S/A49P HICA retains sulfate ion dependence, but with a dissociation constant that indicates a 3-fold tighter binding of anion. This result suggests a significant role for the anion in the escort site, where anion binding may serve to stabilize the R-state conformation and activate the enzyme, regardless of bicarbonate competition.

The structural and functional observations presented here support the revision of our previous hypothesis of a simple (Val47-centered) displacement mechanism for bicarbonate inhibition. We suggest now that a more sophisticated competition between planar (inhibitory) and tetrahedral (activating) anions in the escort site creates a symmetric conformational change tilting helix 3, rearranging the activation loop, burying a new hydrophobic core with the sometimes unstructured N-terminal helices, and capping the active site with the dimer-exchanged N-terminal loops. Indeed, activation by sulfate ion is supported by our observations of the P48S/A49P structure, which allow us to trace the pathway of allosteric communication from the escort site position at the dimer interface to the active site, where the hydrogen-bond network created around Arg46 potentially stabilizes the outward rotation of Asp44 away from the catalytic metal and recruits all critical catalytic residues to the active site.

The role of the escort site for ingress/egress of bicarbonate ion also explains the allosteric response of HICA to bicarbonate binding; enough similarity of ions would allow bicarbonate to compete with the equilibrium association of sulfate or phosphate at the anion binding site, but a lower association of helix 3 with the decreased ionic charge and less ideal steric shape would open up a route to the allosteric pocket, allowing bicarbonate to displace Val47, break the hydrogen-bond contact between Arg46 and Lys51, and attract Tyr181 into the allosteric site to create no less than 8 hydrogen-bonding contacts. The absence of any ion in the escort site in this state allows a shift of helix 3 away from the active site, destabilizing the association with the dimer's N-terminus, and uncapping the active site. With the hydrogen-bond network anchored by Arg46 broken, Asp44 will reassociate with the Zn^{2+} ion as a ligand in the T-state.

This pathway for allosteric communication in HICA provides a plausible rationale for the high salt dependence of activity in HICA, but it does not explain sulfate dependence in particular, which is unlikely to be present in biological systems in millimolar concentrations. The answer to the anion identity question may lie in the documented poor discrimination in enzymes between tetrahedral anions like sulfate and phosphate, the latter of which is estimated to be reasonably present in millimolar concentrations in cells with particularly high ATP use.

CONCLUSIONS

H. influenzae β-carbonic anhydrase (HICA) is an allosteric protein regulated by the binding of bicarbonate ion to a noncatalytic site connected via an activation loop to the inhibitory ligation of Asp44 to the catalytically essential zinc ion. We report here the X-ray crystallographic structures of three activation loop variants (W39V/G41A, P48S/A49P, and W39V/G41A/P48S/A49P) identified based on a comparison of HICA to the crystal structure of the nonallosteric *P. sativum* β-carbonic anhydrase. We found a dissociation of the activation loop state from the active site state, exemplified by the double mutation of W39V/G41A, where the crystal structure revealed Val47 flipped into the allosteric site, consistent with PSCA structure, but an active site very similar to the universally T-state wild-type HICA oligomer. The X-ray crystal structure of a variant with proline shifted from 48 to 49 (P48S/A49P), by contrast, reveals that it has adopted an active site conformation nearly identical to that of nonallosteric β-carbonic anhydrases R-state for one chain, including a tightly associated hydrophobic packing with the dimer-exchanged N-terminal helices; the second chain in the asymmetric unit is associated in a biologically relevant oligomer, but it adopts a T-state conformation not visibly associated with the exchanged helices. We propose that this N-terminal helix association change as a result of anion binding in the escort site is a possible pathway for allosteric communication in HICA. The cooperative link between dimers through the escort/anion binding site suggests a structural discrimination between bicarbonate and sulfate/phosphate ions bound there to functionally influence the packing of the N-termini via the orientation of helix 3. Our kinetic, structural, and spectroscopic studies presented here support a pathway for HICA allosteric and cooperative communication traveling between an anion bridge in the dimerization interface, through the flexible association of the N-terminal dimer-exchanged helices in a hydrophobic core, to the zinc-bound active site.

ASSOCIATED CONTENT

Accession Codes

Coordinates and structure factors have been deposited in the Protein Data Bank as entries 4WAJ, 4WAK, and 4WAM.

AUTHOR INFORMATION

Corresponding Author

*E-mail: rrowlett@colgate.edu; Phone: (315) 228-7245; Fax: (315) 228-7935.

Funding

This work was supported in part by grants (to R.S.R.) from the National Science Foundation (MCB-0741396, MCB-1157332, and CHE-0819686)

Notes

The authors declare no competing financial interest.

ACKNOWLEDGMENTS

The authors gratefully acknowledge Brian J. Bender and Kenneth C. Schmidt for purification and crystallization of protein related to this work.

ABBREVIATIONS

CA, carbonic anhydrase; HICA, *Haemophilus influenzae* β-carbonic anhydrase; ECCA, *Escherichia coli* β-carbonic anhydrase; EDTA, *N*,*N*,*N*′,*N*′-ethylenediaminetetraacetic acid; EXAFS, extended X-ray absorption fine structure spectroscopy; ICP-OES, inductively coupled plasma-optical emission spectroscopy; PCR, polymerase chain reaction; PEG-400, poly(ethylene glycol) 400; HEPES, 4-(2-hydroxyethyl)-piperazineethanesulfonic acid; MOPS, 3-(*N*-morpholino)-

DOI: 10.1021/bi501116e
Biochemistry 2015, 54, 598−611

propanesulfonic acid; CHES, 2-(cyclohexylamino)-ethanesulfonic acid; Bicine, *N*,*N*-bis(2-hydroxyethyl)glycine

REFERENCES

(1) Hewett-Emmett, D. (2000) Evolution and distribution of the carbonic anhydrase gene families. *EXS 90*, 29−76.

(2) Smith, K. S., Jakubzick, C., Whittam, T. S., and Ferry, J. G. (1999) Carbonic anhydrase is an ancient enzyme widespread in prokaryotes. *Proc. Natl. Acad. Sci. U.S.A. 96*, 15184−15189.

(3) Alber, B. E., and Ferry, J. G. (1994) A carbonic anhydrase from the archaeon *Methanosarcina thermophila*. *Proc. Natl. Acad. Sci. U.S.A. 91*, 6909−6913.

(4) Roberts, S. B., Lane, T. W., and Morel, F. M. M. (1997) Carbonic anhydrase in the marine diatom *Thalassiosira weissflogii* (Bacillariophyceae). *J. Phycol. 33*, 845−850.

(5) Lane, T. W., Saito, M. A., George, G. N., Pickering, I. J., Prince, R. C., and Morel, F. M. (2005) Biochemistry: a cadmium enzyme from a marine diatom. *Nature 435*, 42.

(6) Syrjanen, L., Tolvanen, M., Hilvo, M., Olatubosun, A., Innocenti, A., Scozzafava, A., Leppiniemi, J., Niederhauser, B., Hytonen, V. P., Gorr, T. A., Parkkila, S., and Supuran, C. T. (2010) Characterization of the first beta-class carbonic anhydrase from an arthropod (*Drosophila melanogaster*) and phylogenetic analysis of beta-class carbonic anhydrases in invertebrates. *BMC Biochem. 11*, 28.

(7) Burghout, P., Cron, L. E., Gradstedt, H., Quintero, B., Simonetti, E., Bijlsma, J. J. E., Bootsma, H. J., and Hermans, P. W. M. (2010) Carbonic anhydrase is essential for *Streptococcus pneumoniae* growth in environmental ambient air. *J. Bacteriol. 192*, 4054−4062.

(8) Tripp, B. C., Bell, C. B., Cruz, F., Krebs, C., and Ferry, J. G. (2004) A role for iron in an ancient carbonic anhydrase. *J. Biol. Chem. 279*, 6683−6687.

(9) Xu, Y., Feng, L., Jeffrey, P. D., Shi, Y. G., and Morel, F. M. M. (2008) Structure and metal exchange in the cadmium carbonic anhydrase of marine diatoms. *Nature 452*, 56−U53.

(10) Alber, B. E., Colangelo, C. M., Dong, J., Staalhandske, C. M. V., Baird, T. T., Tu, C., Fierke, C. A., Silverman, D. N., Scott, R. A., and Ferry, J. G. (1999) Kinetic and spectroscopic characterization of the gamma-carbonic anhydrase from the methanoarchaeon *Methanosarcina thermophila*. *Biochemistry 38*, 13119−13128.

(11) Barzi, D., Bertini, I., Luchinat, C., and Scozzafava, A. (1979) The electronic spectra of cobalt(II) bovine carbonic anhydrase. *Inorg. Chim. Acta 36*, L431−L432.

(12) Bertini, I. (1980) The spectroscopic investigation of a metalloprotein through metal substitution: carbonic anhydrase. *Mol. Spectrosc., Main Lect. Natl. Conf., 9th*, 46−53.

(13) Kogut, K. A., and Rowlett, R. S. (1987) A comparison of the mechanisms of carbon dioxide hydration by native and cobalt^{2+}-substituted carbonic anhydrase II. *J. Biol. Chem. 262*, 16417−16424.

(14) Lane, T. W., and Morel, F. M. M. (2000) Regulation of carbonic anhydrase expression by zinc, cobalt, and carbon dioxide in the marine diatom *Thalassiosira weissflogii*. *Plant Physiol. 123*, 345−352.

(15) Lindskog, S. (1970) Cobalt(II) in metalloenzymes. A reporter of structure-function relations. *Struct. Bonding (Berlin, Ger.) 8*, 153−196.

(16) Hoffmann, K. M., Samardzic, D., Heever, K. V., and Rowlett, R. S. (2011) Co(II)-substituted *Haemophilus influenzae* beta-carbonic anhydrase: spectral evidence for allosteric regulation by pH and bicarbonate ion. *Arch. Biochem. Biophys. 511*, 80−87.

(17) Cronk, J. D., Rowlett, R. S., Zhang, K. Y. J., Tu, C. K., Endrizzi, J. A., Lee, J., Gareiss, P. C., and Preiss, J. R. (2006) Identification of a novel noncatalytic bicarbonate binding site in eubacterial beta-carbonic anhydrase. *Biochemistry 45*, 4351−4361.

(18) Covarrubias, A. S., Larsson, A. M., Hogbom, M., Lindberg, J., Bergfors, T., Bjorkelid, C., Mowbray, S. L., Unge, T., and Jones, T. A. (2005) Structure and function of carbonic anhydrases from *Mycobacterium tuberculosis*. *J. Biol. Chem. 280*, 18782−18789.

(19) Kimber, M. S., and Pai, E. F. (2000) The active site architecture of *Pisum sativum* beta-carbonic anhydrase is a mirror image of that of alpha-carbonic anhydrases. *EMBO J. 19*, 1407−1418.

(20) Mitsuhashi, S., Mizushima, T., Yamashita, E., Yamamoto, M., Kumasaka, T., Moriyama, H., Ueki, T., Miyachi, S., and Tsukihara, T. (2000) X-ray structure of beta-carbonic anhydrase from the red alga, *Porphyridium purpureum*, reveals a novel catalytic site for CO_2 hydration. *J. Biol. Chem. 275*, 5521−5526.

(21) Strop, P., Smith, K. S., Iverson, T. M., Ferry, J. G., and Rees, D. C. (2001) Crystal structure of the "cab"-type beta class carbonic anhydrase from the archaeon *Methanobacterium thermoautotrophicum*. *J. Biol. Chem. 276*, 10299−10305.

(22) Cox, E. H., McLendon, G. L., Morel, F. M. M., Lane, T. W., Prince, R. C., Pickering, I. J., and George, G. N. (2000) The active site structure of *Thalassiosira weissflogii* carbonic anhydrase 1. *Biochemistry 39*, 12128−12130.

(23) Rowlett, R. S., Hoffmann, K. M., Failing, H., Mysliwiec, M. M., and Samardzic, D. (2010) Evidence for a bicarbonate "escort" site in *Haemophilus influenzae* beta-carbonic anhydrase. *Biochemistry 49*, 3640−3647.

(24) Rowlett, R. S., Tu, C., Lee, J., Herman, A. G., Chapnick, D. A., Shah, S. H., and Gareiss, P. C. (2009) Allosteric site variants of *Haemophilus influenzae* β-carbonic anhydrase. *Biochemistry 48*, 6146−6156.

(25) Rowlett, R. S. (2010) Structure and catalytic mechanism of the beta-carbonic anhydrases. *Biochim. Biophys. Acta, Proteins Proteomics 1804*, 362−373.

(26) Rowlett, R. S. (2014) Structure and catalytic mechanism of beta-carbonic anhydrases. *Subcell. Biochem. 75*, 53−76.

(27) Rowlett, R. S., Tu, C., McKay, M. M., Preiss, J. R., Loomis, R. J., Hicks, K. A., Marchione, R. J., Strong, J. A., Donovan, G. S., and Chamberlin, J. E. (2002) Kinetic characterization of wild-type and proton transfer-impaired variants of beta-carbonic anhydrase from *Arabidopsis thaliana*. *Arch. Biochem. Biophys. 404*, 197−209.

(28) Johansson, I. M., and Forsman, C. (1993) Kinetic studies of pea carbonic anhydrase. *Eur. J. Biochem. 218*, 439−446.

(29) Johansson, I. M., and Forsman, C. (1994) Solvent hydrogen isotope effects and anion inhibition of CO_2 hydration catalysed by carbonic anhydrase from *Pisum sativum*. *Eur. J. Biochem. 224*, 901−907.

(30) Smith, K. S., Cosper, N. J., Stalhandske, C., Scott, R. A., and Ferry, J. G. (2000) Structural and kinetic characterization of an archaeal beta-class carbonic anhydrase. *J. Bacteriol. 182*, 6605−6613.

(31) Rowlett, R. S., Chance, M. R., Wirt, M. D., Sidelinger, D. E., Royal, J. R., Woodroffe, M., Wang, Y.-F. A., Saha, R. P., and Lam, M. G. (1994) Kinetic and structural characterization of spinach carbonic anhydrase. *Biochemistry 33*, 13967−13976.

(32) Monod, J., Wyman, J., and Changeux, J.-P. (1965) On the nature of allosteric transitions: a plausible model. *J. Mol. Biol. 12*, 88−118.

(33) Rowlett, R. S., Tu, C., Murray, P. S., and Chamberlin, J. E. (2004) Examination of the role of Gln-158 in the mechanism of CO_2 hydration catalyzed by beta-carbonic anhydrase from *Arabidopsis thaliana*. *Arch. Biochem. Biophys. 425*, 25−32.

(34) Covarrubias, A. S., Bergfors, T., Jones, T. A., and Hoegbom, M. (2006) Structural mechanics of the pH-dependent activity of beta -carbonic anhydrase from *Mycobacterium tuberculosis*. *J. Biol. Chem. 281*, 4993−4999.

(35) Sarkar, G., and Sommer, S. S. (1990) The megaprimer method of site-directed mutagenesis. *BioTechniques 8*, 404−407.

(36) Miyazaki, K., and Takenouchi, M. (2002) Creating random mutagenesis libraries using megaprimer PCR of whole plasmid. *BioTechniques 33*, 1036−1038.

(37) Khalifah, R. G. (1971) Carbon dioxide hydration activity of carbonic anhydrase. I. Stop-flow kinetic studies on the native human isoenzymes B and C. *J. Biol. Chem. 246*, 2561−2573.

(38) Ghannam, A. F., Tsen, W., and Rowlett, R. S. (1986) Activation parameters for the carbonic anhydrase II-catalyzed hydration of carbon dioxide. *J. Biol. Chem. 261*, 1164−1169.

(39) Rowlett, R. S., Gargiulo, N. J., III, Santoli, F. A., Jackson, J. M., and Corbett, A. H. (1991) Activation and inhibition of bovine carbonic anhydrase III by dianions. *J. Biol. Chem. 266*, 933−941.

DOI: 10.1021/bi501116e
Biochemistry 2015, 54, 598−611

(40) (2011) *CrysAlisPro*, version 1.171.34.49, Agilent Technologies UK Ltd, Oxford, UK.
(41) Evans, P. (2006) Scaling and assessment of data quality. *Acta Crystallogr., Sect. D: Biol. Crystallogr. 62*, 72−82.
(42) McCoy, A. J., Grosse-Kunstleve, R. W., Adams, P. D., Winn, M. D., Storoni, L. C., and Read, R. J. (2007) Phaser crystallographic software. *J. Appl. Crystallogr. 40*, 658−674.
(43) Murshudov, G. N., Vagin, A. A., and Dodson, E. J. (1997) Refinement of macromolecular structures by the maximum-likelihood method. *Acta Crystallogr., Sect. D: Biol. Crystallogr. 53*, 240−255.
(44) Emsley, P., and Cowtan, K. (2004) Coot: model-building tools for molecular graphics. *Acta Crystallogr., Sect. D: Biol. Crystallogr. 60*, 2126−2132.
(45) Emsley, P., Lohkamp, B., Scott, W. G., and Cowtan, K. (2010) Features and development of Coot. *Acta Crystallogr., Sect. D: Biol. Crystallogr. 66*, 486−501.
(46) Winn, M. D., Isupov, M. N., and Murshudov, G. N. (2001) Use of TLS parameters to model anisotropic displacements in macromolecular refinement. *Acta Crystallogr., Sect. D: Biol. Crystallogr. 57*, 122−133.
(47) Engh, R. A., and Huber, R. (1991) Accurate bond and angle parameters for X-ray protein structure refinement. *Acta Crystallogr., Sect. A 47*, 392−400.

DOI: 10.1021/bi501116e
Biochemistry 2015, 54, 598−611